Jérôme Garot, MD, PhD
João A. C. Lima, MD
Bernhard L. Gerber, MD, PhD
Smita Sampath, MS
Kathy C. Wu, MD
David A. Bluemke, MD, PhD
Jerry L. Prince, PhD
Nael F. Osman, PhD

Index terms:
Heart, MR, 511.121412, 511.12143
Magnetic resonance (MR), comparative studies
Magnetic resonance (MR), contrast enhancement, 511.12143
Myocardium, infarction, 511.814

Published online
10.1148/radiol.2332031676
Radiology 2004; 233:596–602

Abbreviations:
E_{ll} = longitudinal strain
DTPA = diethylenetriaminepentaacetic acid
LV = left ventricular
MI = myocardial infarction
3D = three-dimensional

[1] From the Department of Medicine, Division of Cardiology (J.G., J.A.C.L., B.L.G., K.C.W.), Department of Electrical Engineering (S.S., J.L.P., N.F.O.), and Department of Radiology (D.A.B., N.F.O.), Johns Hopkins University, Baltimore, Md. Received October 15, 2003; revision requested January 8, 2004; revision received January 12; accepted February 2. Supported by NIH/NHLBI grants R29HL-47405, HL-4590, and N01-HC95162. J.G. supported by a Boehringer-Ingelheim grant of the Fédération Française de Cardiologie (Reims, France). **Address correspondence to** J.G., Henri Mondor University Hospital, Cardiologie 8ème, 51 Avenue du Maréchal de Lattre de Tassigny, 94010 Créteil, France (e-mail: *jgarot@free.fr*).

Author contributions:
Guarantors of integrity of entire study, J.G., N.F.O.; study concepts, J.G., J.A.C.L., B.L.G., J.L.P., N.F.O.; study design, J.G., J.A.C.L., J.L.P., N.F.O.; literature research, J.G., N.F.O., J.A.C.L.; clinical studies, J.G., J.A.C.L., B.L.G., K.C.W., D.B.; experimental studies, J.G., S.S., J.L.P., N.F.O.; data acquisition, J.G., J.A.C.L., B.L.G., K.C.W., D.B., N.F.O.; data analysis/interpretation, J.G., B.L.G., K.C.W., N.F.O., S.S.; statistical analysis, J.G., B.L.G., S.S.; manuscript preparation, J.G., J.A.C.L., N.F.O., J.L.P., K.C.W.; manuscript definition of intellectual content, J.G., J.A.C.L., N.F.O., J.L.P.; manuscript editing, J.G., N.F.O.; manuscript revision/review, J.G., J.A.C.L., J.L.P., N.F.O., B.L.G., S.S.; manuscript final version approval, all authors

Spatially Resolved Imaging of Myocardial Function with Strain-encoded MR: Comparison with Delayed Contrast-enhanced MR Imaging after Myocardial Infarction

Strain-encoded magnetic resonance (MR) imaging was prospectively evaluated for direct imaging of systolic myocardial strain and compared with cross-registered delayed contrast material–enhanced MR imaging in five healthy volunteers and nine patients with infarction. Local contractile performance was decreased in infarcted myocardium versus that in remote and adjacent myocardium ($P < .01$) and in adjacent versus remote myocardium ($P < .05$). The extent of dysfunctional myocardium, as assessed with strain-encoded MR imaging, was greater than that of hyperenhancement, as assessed with delayed contrast-enhanced MR imaging ($P < .05$). Strain values obtained with strain-encoded MR imaging were strongly correlated with those obtained with three-dimensional tagged MR imaging ($r = 0.75$, $P < .001$). Strain-encoded MR imaging provides spatially resolved (1.5 × 2.5-mm) imaging and measurement of myocardial strain in humans without the need for postprocessing, which may improve routine comprehensive evaluation of myocardial viability.

The detection of myocardial viability has important therapeutic and prognostic implications in patients with acute myocardial infarction (MI) or chronic ischemic left ventricular (LV) dysfunction (1–3). The assessment of local inotropic reserve with stress echocardiography (4,5) and myocardial perfusion with scintigraphy (6) is used routinely in the clinical assessment of myocardial viability. Ideally, accurate determination of local viability requires comprehensive assessment of the extent of ischemic tissue damage, along with detailed information on segmental LV function to enable more accurate prediction of functional recovery. By providing detailed assessment of regional LV function at rest and with administration of dobutamine (7,8), or more recently, by allowing direct imaging of irreversibly damaged myocardium (9,10), magnetic resonance (MR) imaging has emerged as the technique that could provide accurate determination of local myocardial viability. However, obtaining detailed three-dimensional (3D) images of myocardial strain requires tedious offline postprocessing of tagged images (11–13).

In contrast to conventional tagging, strain-encoded MR imaging is a technique that uses tag surfaces that are parallel, not orthogonal, to the image plane, combined with out-of-plane phase-encoding gradients in the perpendicular section-select direction (14). Because local frequency of the tag pattern is related to myocardial strain (15,16), we hypothesized that strain-encoded MR imaging might provide direct myocardial longitudinal strain (E_{ll}) imaging embedded on short-axis images of the LV. This technique may have potential in the online

assessment of intrinsic myocardial contractility and may therefore represent a powerful addition to the assessment of myocardial viability by quantifying local function automatically. Thus, the purpose of our study was to prospectively evaluate strain-encoded MR imaging as a method for direct imaging of regional LV function that precludes the need for postprocessing and can be used in combination with contrast material–enhanced MR imaging in the assessment of local myocardial viability.

Materials and Methods

Study Population

Over a 3-month period, 28 patients admitted for acute MI were consecutively screened. To be included, patients had to have symptoms of a first-time acute MI, no history of coronary artery disease or other cardiac disease, single-vessel coronary disease with a clearly identified culprit artery, and no contraindication to MR imaging. Nine patients with MI (two women and seven men; mean age, 56 years ± 10; five with anterior MI and four with inferior MI; mean peak creatine kinase level ± standard deviation, 2150 IU ± 450) were included. The diagnosis of infarction was confirmed with coronary angiography and by the presence of chest pain, ST segment elevation of more than 1 mm in at least two contiguous leads at electrocardiography, and substantial elevation of creatine kinase-MB isoenzymes (more than twice the highest normal value). All patients underwent successful (residual stenosis of less than 30%, Thrombolysis in Myocardial Infarction trial grade 3 flow) direct coronary angioplasty of the culprit vessel (left anterior descending coronary artery in five patients and right coronary artery in four) 3 hours ± 2 after the onset of chest pain, along with stent implantation (n = 1.2 stents per patient). Five healthy volunteers (one woman and four men; mean age, 30 years ± 4; $P < .05$) with no history of cardiac disease and normal findings at physical examination were also included. The study protocol was approved by the Joint Committee on Clinical Investigation of the Johns Hopkins Medical Institutions. Written informed consent was obtained from all patients and volunteers.

Data Acquisition

Clinical research studies were performed with a 1.5-T MR imager (Signa; GE Medical Systems, Milwaukee, Wis). Anterior and posterior phased-array surface coils were used for signal acquisition. Strain-encoded MR images and 3D tagged MR images, which were used as a reference for measurement of myocardial strain, were acquired sequentially in all subjects. In addition, gadolinium (Gd) diethylenetriaminepentaacetic acid (DTPA)–enhanced MR imaging was performed in patients with MI who underwent cardiac MR imaging 3 days ± 1 after acute MI.

Strain-encoded MR imaging.—Strain-encoded MR imaging uses tag planes parallel and not orthogonal to the LV short-axis image plane. We used a modified 1–1 spatial modulation of magnetization tagging pulse sequence with a magnetic field gradient oriented in the section direction to spatially modulate the longitudinal magnetization in a sinusoidal pattern, so that planes of constant sinusoidal phase are parallel to the image plane. During systole, the healthy human LV undergoes displacement and deformation along its long axis (longitudinal direction). The tag pattern moves with the tissue and undergoes compression, while the LV shortens along the long axis. Thus, myocardial tissue strain affects the frequency of the tag pattern locally. More specifically, myocardial E_{ll} is proportional to the local frequency vector of the tag pattern in the longitudinal (z) direction.

Strain-encoded MR imaging is used to measure the frequency and orientation of the tag pattern within each voxel and provides all that is needed to calculate a high-resolution map of Eulerian E_{ll} on a short-axis section (14). Strain is defined as the change in length per unit length. To measure the local frequency within each voxel, we used a modified electrocardiographically triggered segmented k-space fast gradient-echo imaging pulse sequence (17). From the long-axis scout image, we prescribed three equidistant sections that spanned the entire LV. Out-of-plane 1–1 SPAMM tags with a tag period of 2.5 mm were applied at end diastole, parallel to the image plane, and a phase-encoding gradient (G_z)—which we call the tuning gradient—was applied in the z direction (section-select direction) before readout. For measurement of E_{ll}, the method requires acquisition of two images per location corresponding to two different tuning gradients orthogonal to the image plane. The selected tuning values depend on initial tag separation and expected changes in tag frequency as a result of regional tissue shortening. Tag frequency corresponds mathematically to the reciprocal of tag separation. We chose a tag separation of 2.5 mm, which corresponds to a 0.40-mm^{-1} tag frequency. Since we expected maximal systolic longitudinal shortening to be about 15%, the corresponding tag frequency was 0.46 mm^{-1}. These two tuning values (0.40 and 0.46 mm^{-1}), chosen to correspond to a 0%–15% range of strain values (14), were applied at each section location (one per breath hold) (Fig 1). From these two images, a strain image was automatically produced, of which signal intensity is directly related to E_{ll} (Appendix). Typical imaging parameters were a 400-mm field of view; 10-mm section thickness; 256 × 160 matrix; repetition time msec/echo time msec, 6.8/1.8; flip angle, 20°; one signal acquired; and 1.56 × 2.50-mm in-plane resolution. Breath-hold time was about 10 seconds. This sequence was used to generate five to seven images throughout systole with a temporal resolution of about 50 msec.

Conventional 3D tagged MR imaging.—An electrocardiographically triggered segmented k-space fast gradient-echo imaging pulse sequence was used (17). The tagging pulse sequence consisted of nonselective radiofrequency pulses separated by spatial modulation of magnetization encoding gradients to achieve a tag separation of 7 mm. After scout images were obtained, contiguous stacks of five base-to-apex short-axis cross sections were prescribed. Two sets of identical one-dimensional tagged short-axis views were acquired (the second set was rotated 90°). This imaging sequence allowed us to acquire five sections within five breath holds of about 12–16 seconds. From the most basal section, six equidistant radially oriented (every 30°) long-axis sections were prescribed. Imager settings were as follows: 360-mm field of view, 7-mm tag separation, 8-mm section thickness, 6.5/2.3, 15° flip angle, 256 × 160 matrix, and between five and seven phase-encoded views obtained throughout systole.

Delayed Gd-DTPA–enhanced MR imaging.—Gd-DTPA–enhanced MR imaging has been used to characterize acute MI and represents an accepted technique for infarct delineation in humans (9,10). Because of the increased volume of distribution and altered wash-in and washout kinetics of the extravascular contrast agent within infarcted myocardium, images acquired 10–15 minutes after contrast agent injection demonstrate regional hyperenhancement in the infarcted area relative to the remote area. After conventional 3D tagging and strain-encoded acquisitions were completed, images were acquired 10–15 minutes after administra-

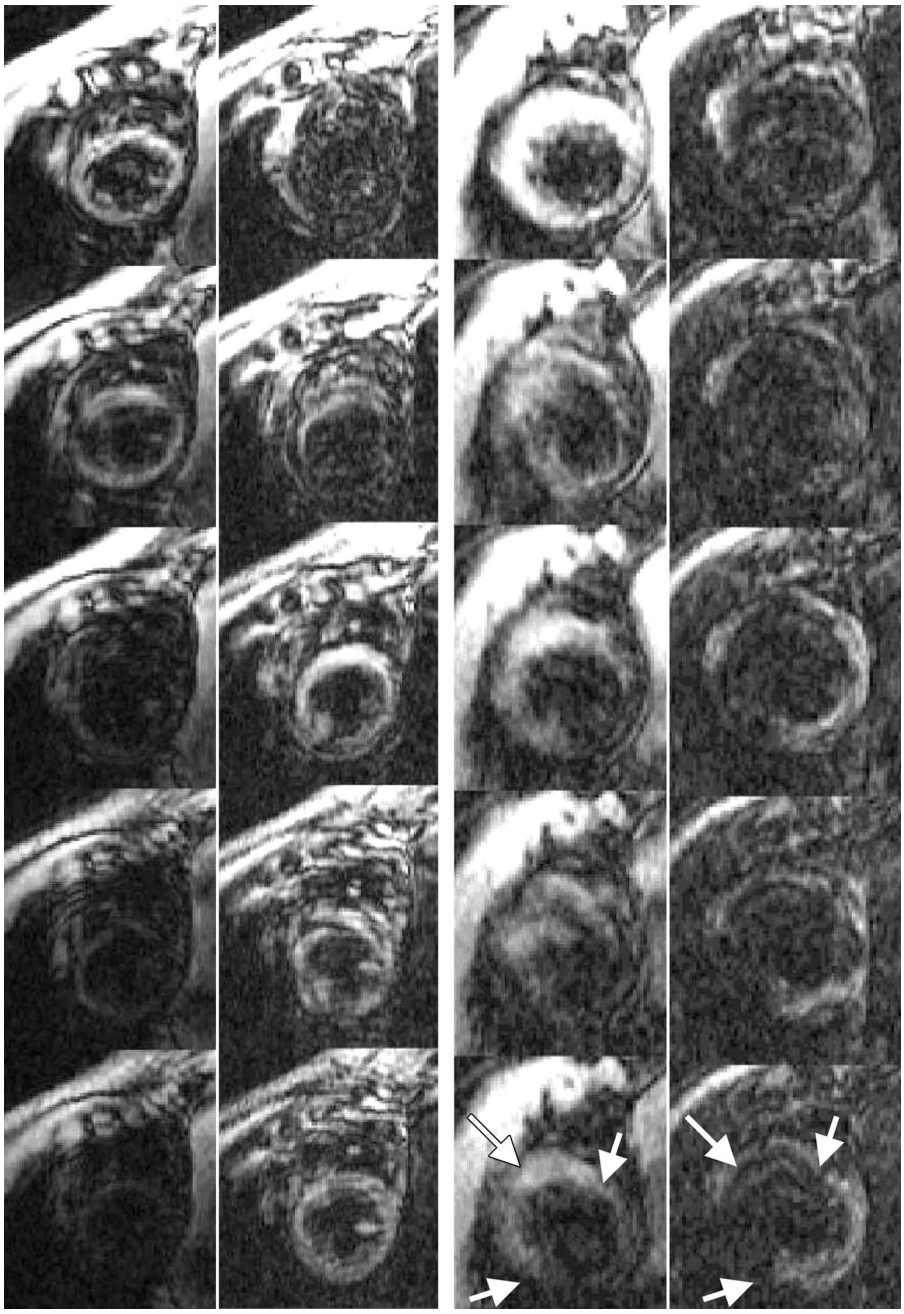

Figure 1. Phase-encoded images obtained with strain-encoded MR imaging throughout systole (from top to bottom, 55-msec resolution time) in a healthy subject (left panel) and a patient with recent anterior MI (right panel), with 0.40-mm^{-1} and 0.46-mm^{-1} tuning values, respectively. With tuning of 0.40 mm^{-1}, the myocardium appears bright on the first image during systole, and this signal disappears progressively throughout systole; this is indicative of myocardial longitudinal shortening in the normally contracting myocardium. In contrast, with tuning of 0.46 mm^{-1}, the myocardium is initially dark, and then the contracting myocardium becomes progressively brighter throughout systole. At end-systole, the two phase-encoded images are homogeneous in the healthy subject, whereas the anterior dysfunctional region is clearly seen in the patient with infarction (arrows).

tion of an intravenous bolus of 0.1 mmol/kg Gd-DTPA (Omniscan; Sanofi-Synthélabo, Paris, France). We prescribed six short-axis sections spanning the entire LV from base to apex. We used an inversion-recovery prepared fast spoiled gradient-echo pulse sequence with an inversion time between the 180° inversion-recovery pulse and the radiofrequency imaging pulse of 200–270 msec (250–270 msec in eight patients and 200 msec in one), which was found to provide optimal contrast between remote and infarcted myocardium. Imaging parameters were as follows: 256 × 192 image matrix, 6.0/2.3, 360-mm field of view, 7-mm section thickness, and 20° flip angle. Each section was acquired in a single breath hold of about 8–10 seconds. Mean total time spent in the imager for a patient was about 45 minutes.

Data Analysis

Strain-encoded MR imaging.—Two short-axis images with two different tuning values in the direction orthogonal to the image plane were acquired at each section location. From these images, a dense map of E_{ll} was automatically generated by using a mathematic equation, as described in the Appendix. On this strain image, coordinates of the posterior right ventricular–LV insertion point were calculated on the most basal section and used as reference landmarks for segmentation of the LV into five segments: inferior, inferolateral, lateral, anterior, and septal wall. For each short-axis section of the heart, the same five-segment model was then applied for cross-registration between imaging modalities, and mean maximal E_{ll} (five points per segment) was automatically computed at end systole in the subendocardium and subepicardium of each myocardial segment at the base, middle LV, and apex. E_{ll} depends directly on the intensity of the E_{ll} image and was automatically determined (Appendix). For measurement of maximal systolic strain, the still frame exhibiting maximal deformation at end systole was selected. For assessment of reproducibility, analysis was performed by two independent observers (J.G. and N.F.O., both with 9 years experience in cardiac MR imaging), who were blinded to each other and other data. Also, the area of dysfunctional myocardium was visually assessed on the strain image and manually contoured (J.G.).

Conventional 3D tagged MR imaging.—Maximum myocardial E_{ll} was assessed (B.L.G., 9 years of experience with cardiac MR imaging) off-line at end-systole in the subendocardium and subepicardium by using an established tracking motion technique (13), as previously described (16). Images were processed by using a validated software program that requires interactive and time-consuming detection of myocardial contours and tag lines from short- and long-axis tagged cardiac images to generate a dense motion map (13). E_{ll} was computed at the

base, middle LV, and apex. The time required for a complete quantitative analysis was about 6–8 hours per subject. To ensure adequate cross-registration between strain-encoded, contrast-enhanced, and 3D tagged MR imaging, the three anatomic levels along the LV long axis were automatically copied and acquired with each imaging modality.

Delayed Gd-DTPA–enhanced MR imaging.—The same five-segment model was applied to identical section locations by using the same landmark for cross-registration. Segments were categorized as infarcted or not, on the basis of the presence or absence of hyperenhancement on delayed contrast-enhanced images (J.A.C.L., 15 years of experience with cardiac MR imaging). In each segment, infarct transmurality was determined visually as being more or less than 50% of myocardial wall thickness. For the purpose of analysis, infarctions were considered nontransmural when less than 50% of myocardial wall thickness and transmural when more than 50%. Myocardial segments that were immediately contiguous to the infarct region either radially or longitudinally were labeled as adjacent. Segments that were neither infarcted nor adjacent were categorized as remote. For each segment, the analysis was performed in the subendocardium (inner half) and subepicardium (outer half). Areas of hyperenhancement were contoured manually (J.A.C.L.).

Statistical Analysis

Values are shown as mean and standard error. Comparisons between myocardial strain obtained with strain-encoded MR imaging in remote, infarcted, and adjacent myocardium were assessed with repeated-measures analysis of variance with post-hoc Tukey correction. Comparisons between the two methods for assessment of E_{ll} were performed with the paired Student *t* test. Correlations between the two techniques were assessed with linear regression analysis and Bland-Altman plots. Interobserver reproducibility of strain-encoded MR imaging was assessed with linear regression analysis, and the coefficient of variability between the two series of measurements was computed. Proportions were compared with χ^2 analysis. All tests were two tailed and considered to indicate a statistically significant difference when the *P* value was less than .05.

Results

Strain-encoded MR Images in Healthy Volunteers

In healthy volunteers, maximal systolic deformation obtained with strain-encoded MR imaging was homogeneous at each section location and along the LV long axis, which is in agreement with the concept of homogeneous LV function in this population (Fig 2). For the five volunteers, maximal systolic E_{ll} obtained automatically from strain-encoded MR images was greater in the septum ($-10.6\% \pm 0.5$) and less in the lateral free wall ($-9.5\% \pm 0.4$; $P < .05$, as calculated with post hoc analysis of variance). We observed only moderate variations of E_{ll} from the base to the apex in a given myocardial segment (from $-10.6\% \pm 0.5$ to $-10.1\% \pm 0.4$ in the septum and from $-9.5\% \pm 0.4$ to $-9.1\% \pm 0.4$ in the lateral free wall, $P > .05$).

Strain-encoded MR Imaging versus Delayed Contrast-enhanced MR Imaging

Gd-DTPA-enhanced MR imaging consistently showed regional hyperenhancement in the anterior wall among the five patients with anterior MI and in the inferior wall among the four patients with inferior MI. When contrast-enhanced MR imaging was used for infarction delineation, strain-encoded MR imaging consistently showed decreased E_{ll} (blue color on the strain-encoded image) in infarcted regions relative to remote regions (Fig 3). In all patients, the dysfunctional region on strain-encoded images (blue color, decreased E_{ll}) matched the region of hyperenhancement on delayed contrast-enhanced images. Of 270 analyzed myocardial sectors (135 segments × two layers), 68 were infarcted on contrast-enhanced MR images, and 118 were dysfunctional on strain-encoded MR images (< 2 standard deviations from normal mean in controls in the same sector). By means of planimetry, the mean and standard deviation of the area of hyperenhancement on delayed contrast-enhanced images (percentage of LV surface area) and the extent of dysfunctional myocardium on strain-encoded MR images were 20.0% ± 5.7 (range, 12%–31%) and 28.0% ± 7.2 (range, 18%–39%), respectively ($P < .05$). In six patients, the extent of dysfunctional myocardium, as assessed with strain-encoded MR imaging, was larger than the hyperenhanced region on delayed perfusion images (31.5% ± 5.6 vs 20.2% ± 6.9 of LV surface area, $P < .01$) (Fig 3).

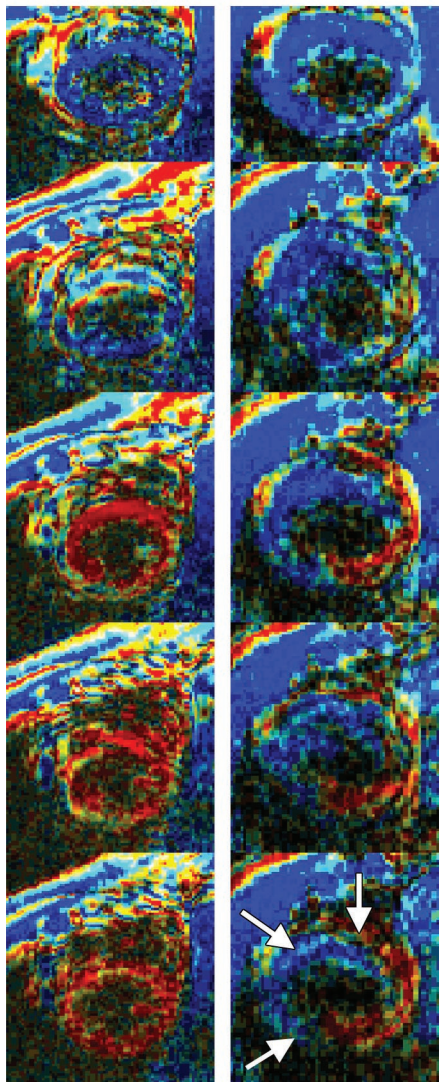

Figure 2. E_{ll} images of the LV throughout systole (successive time frames during R-R interval from top to bottom) in the same healthy subject (left) and patient (right) as in Figure 1. A strain image is produced automatically by combining the two phase-encoded images (Appendix). The dysfunctional myocardium appears blue (arrows) on the strain image, and normally contracting myocardium appears red.

Interobserver reproducibility for measurement of E_{ll} with strain-encoded MR imaging in all patients was good (y, $1.02x - 0.09$; $r = 0.98$; $P < .001$; coefficient of variability, 2%). Among 270 myocardial sectors analyzed with contrast-enhanced MR imaging, 68 were classified as infarcted, 70 as adjacent, and 132 as remote. In infarcted myocardium, E_{ll} was assessed with strain-encoded MR imaging and was decreased relative to ad-

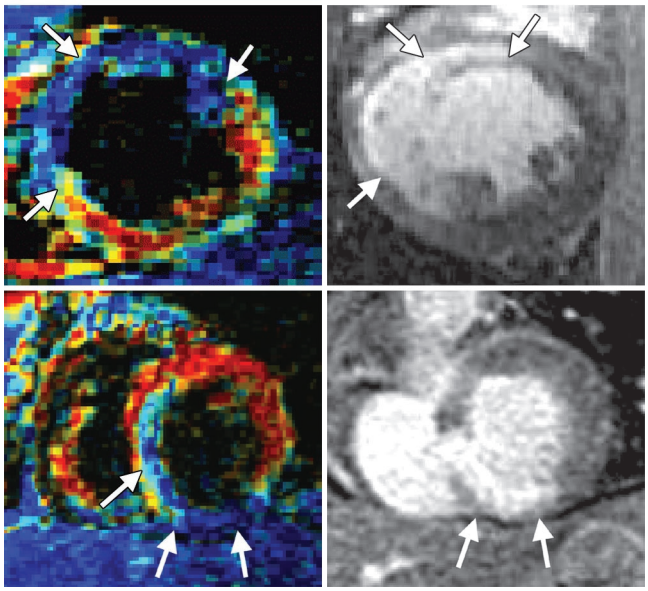

Figure 3. LV E_{ll} images obtained with strain-encoded MR imaging at end-systole (left column) and corresponding delayed Gd-DTPA–enhanced MR images (right column) of patients with anterior (top row) and inferior (bottom row) MIs (arrows). Dysfunctional myocardium appears blue on the strain image, and normally contracting myocardium appears red. Color maps were obtained with use of conventional look-up table from gray-scale images for display purposes.

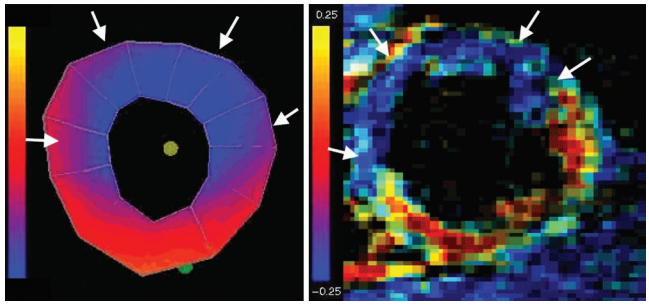

Figure 4. E_{ll} map of the LV obtained with a tracking motion technique from 3D tagged MR images (left) and longitudinal strain image obtained with strain-encoded MR imaging (right) in a patient with anterior MI (arrows). The conventional strain map is produced in about 6–8 hours, whereas strain-encoded MR imaging provides a strain image automatically and instantly without human intervention. Dysfunctional myocardium appears blue on the strain map and strain-encoded image; contracting myocardium is normally red.

jacent myocardium (−3.6% ± 0.2 vs −7.5% ± 0.3, $P < .01$ with repeated post hoc analysis of variance) and remote myocardium (−8.3% ± 0.2, $P < .01$). The LV myocardium adjacent to the infarct territory showed decreased E_{ll} relative to remote myocardium ($P < .05$). E_{ll} was lower in remote myocardium compared with healthy myocardium (−8.3% ± 0.2 vs −9.8% ± 0.1, $P < .01$). Finally, there was a trend toward greater myocardial deformation in patients with nontransmural infarcts (<50% transmural extent, $n = 20$ myocardial segments [ie, 20 subendocardial sectors]) versus patients with transmural infarcts (>50%, $n = 24$ myocardial segments [ie, 48 sectors]) (−4.0% ± 0.4 vs −3.1% ± 0.3, $P = .07$).

Strain-encoded MR Imaging versus Conventional 3D Tagged MR Imaging

Values of maximal systolic E_{ll} obtained directly from strain-encoded MR images and standard 3D tagged MR images are shown in patients with infarction (Table). The concordance between E_{ll} maps as assessed with strain-encoded and conventional 3D tagged MR imaging is illustrated in a patient with anterior MI in Figure 4. For pooled data in patients with infarcted, adjacent, or remote myocardium, there was a good correlation between the two methods for assessment of E_{ll} ($r = 0.75$; standard error, 1.88; $P < .01$; Fig 5a). When comparing individual differences between the two techniques in each segment, we observed slightly lower E_{ll} values with strain-encoded MR imaging at the higher range and slightly higher values at the lower range, as reflected by the Bland-Altman plot (Fig 5b). The time for complete analysis of E_{ll} in a single subject was typically about 6–8 hours with 3D tagged MR imaging and less than 30 seconds with strain-encoded MR imaging. From the two phase-encoded images, a strain image is produced in a fraction of a second (see equations in the Appendix). The LV myocardium is then divided in equally distributed radial sectors, and quantitative data are obtained automatically in about 5 seconds (for time for segmentation of the LV and for calculation of myocardial strain, see Appendix).

Discussion

The results of this study demonstrate the feasibility and accuracy of strain-encoded MR imaging in direct longitudinal shortening strain imaging and measurement of human LV myocardium. We also propose an integrated MR approach, through the use of strain-encoded and delayed contrast-enhanced MR imaging, for online comprehensive assessment of segmental LV contractility and ischemic tissue damage after acute MI. By providing online assessment of regional myocardial deformation with accurate cross-registration with Gd-DTPA-enhanced MR imaging, strain-encoded MR imaging may represent an important addition to the evaluation of myocardial viability. This method is based on the use of tag surfaces parallel to the imaging plane. The local frequency of the tag pattern (ie, through-plane myocardial strain) can be measured throughout systole in each voxel by using two different tuning gradients perpendicular to the image plane. We show that E_{ll} can be imaged from short-axis sections of the LV and that the method allows for accurate transmural assessment of E_{ll} across the wall in infarcted, adjacent, and remote LV myocardium in humans. Quantitative assessment of E_{ll} is produced automatically without the need for additional postprocessing.

Importance of Myocardial Strain in Infarcted, Adjacent, and Remote Myocardium

By using MR tagging in sheep, Kramer et al (18) reported a decrease in circumferential and longitudinal shortening strain in adjacent myocardium relative to remote noninfarcted regions. In human patients, circumferential shortening strain was reduced in remote noninfarcted myocardium in comparison with that in human subjects (19). In dogs, Lima et al (20) reported impaired systolic wall thickening in the nonischemic myocardium immediately adjacent to the ischemic region and, to a lesser degree, in remote

Longitudinal Strain in Infarcted, Adjacent, and Remote Myocardium

Imaging Technique	Infarcted Myocardium (n = 68)		Adjacent Myocardium (n = 70)		Remote Myocardium (n = 132)	
	Subendocardium	Subepicardium	Subendocardium	Subepicardium	Subendocardium	Subepicardium
Strain-encoded MR imaging	−3.9 ± 0.2*†	−3.3 ± 0.3†	−8.2 ± 0.4‡	−6.8 ± 0.4*‡	−8.8 ± 0.3*	−7.7 ± 0.3
3D tagged MR imaging	−2.9 ± 0.5	−2.9 ± 0.5	−8.3 ± 0.6	−5.8 ± 0.6	−9.7 ± 0.4	−7.9 ± 0.4

Note.—Data are mean percentages ± standard error.
* $P < .05$ versus 3D tagged MR imaging (paired Student t test).
† $P < .01$ versus adjacent and remote myocardium (repeated analysis of variance).
‡ $P < .05$ versus remote myocardium (repeated analysis of variance).

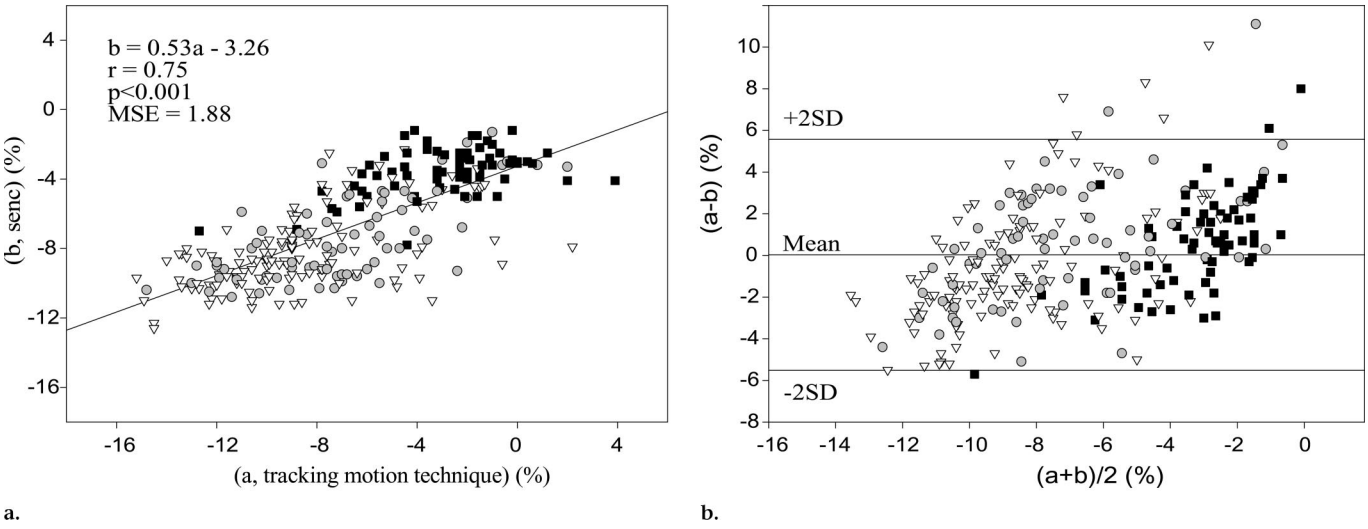

Figure 5. **(a)** Correlation and **(b)** Bland-Altman plots for comparisons of the pooled E_{ll} values obtained with strain-encoded MR imaging (**b**) and a tracking motion technique from 3D tagged MR images (**a**) in patients with MI. Note the good correlation (**a**) and absence of significant and systematic difference (*SD*) (**b**) between strain-encoded and 3D tagged MR imaging derived myocardial strain. ■ = infarcted myocardium. ● = adjacent myocardium. ▽ = remote myocardium.

regions. In concordance with previous findings, we report a decrease in longitudinal shortening strain in adjacent myocardium after acute MI, as compared with that of remote myocardium. We also report a decrease in tissue strain in remote myocardium early after acute MI versus tissue strain in the same segments in control subjects. The regional dysfunction in adjacent and remote myocardium may be due to increased wall stress or mechanical tethering to infarcted regions and may be an important determinant of LV remodeling after MI (18–20). Moreover, by depicting subtle differences in regional function within ischemic, adjacent, and remote myocardium, strain-encoded MR imaging enables a detailed assessment of LV mechanics during LV postinfarct remodeling.

Advantages

The technique provides direct imaging and assessment of E_{ll} and permits complete bypass of tedious interactive tracking of LV contours and tag motion over time from both short- and long-axis tagged images. In addition, tracking motion techniques with 3D tagged MR imaging require the use of complex algorithms to reconstruct a 3D strain tensor. A dense strain map is produced with interpolation and averaging. Fusing of short- and long-axis data requires careful registration, which may be altered by patient movement over a long series of breath holds. In contrast, strain-encoded MR imaging provides greater spatial resolution for pixel-by-pixel assessment of myocardial strain.

It has been shown that accurate information about tag motion and tissue deformation can be obtained from one spectral peak in k space for each direction of tag line (15,16). The development of a fast imaging pulse sequence with limited k-space acquisition may have potential for real-time strain-encoded MR imaging. This would be of great importance for real-time quantitative monitoring of regional LV function during cardiac stress MR imaging.

Limitations

This work does not provide new pathophysiologic insights, but its aim was to present initial validation of an attractive and direct strain imaging and measurement technique. Three sections were acquired per patient, but there is no technical limitation for the number of sections one can acquire with strain-encoded MR imaging. The complex mechanics of the LV are best described when myocardial strain can be assessed in various directions. If used in combination with harmonic-phase MR imaging (16), which provides detailed assessment of two-dimensional myocardial strain in the circumferential and radial directions, the automated detailed assessment of 3D cardiac mechanics can be implemented in humans. Maximal systolic strain was measured for validation purposes, but strain-encoded MR imaging enables determina-

tion of myocardial strain at each phase during systole, with a temporal resolution of about 50 msec. However, tag fading during diastole, along with 50-msec temporal resolution, did not allow for robust and accurate assessment of postsystolic thickening.

The two tuning values used in this study were predetermined on the basis of the normal range of E_{ll} in healthy subjects. Comparison with 3D tagged MR imaging shows slightly lower strain values with strain-encoded MR imaging at the higher range and slightly higher values at the lower range. However, differences between the two modalities are moderate at the extreme range of values (absolute difference in longitudinal shortening strain is <4% in more than 95% of patients). This indicates that slight variations in tuning values have only moderate impact on strain measurement. The method requires two short breath holds per location, but the total acquisition time for assessment of E_{ll} is substantially reduced, since long-axis sections of the heart are not needed. Although quantitative myocardial strain imaging may provide more information than visual assessment, the clinical relevance of the technique remains to be formally demonstrated.

Strain-encoded MR imaging provides direct spatially resolved imaging and quantification of myocardial E_{ll} in humans without the need for additional time-consuming postprocessing. In patients with acute MI, we believe on-line quantification of regional LV contractility may represent an important addition to the evaluation of ischemic myocardial damage with contrast-enhanced MR imaging. We also believe this integrated approach has great potential for improved comprehensive evaluation of local myocardial viability.

Appendix

Strain-encoded MR Images

To image the local frequencies of the voxels (14), a gradient $G_T(\tau)$ is applied in the section-select or z direction, which corresponds to a tuning frequency in the z direction by using the following equation:

$$\omega_T = \gamma \int G_T(\tau) d\tau.$$

The resulting image (I) is the integral in the z direction of the longitudinal magnetization (M), multiplied by the tuning frequency factor over the section profile (s), as follows:

$$I(x,y,t;\omega_T) = \int_{-\infty}^{\infty} M(x,y,z,t)s(z)e^{-j\omega_T z}dz.$$

Two images are acquired: $I_L(x,y,t) = I(x,y,t;\omega_L)$ and $I_H(x,y,t) = I(x,y,t;\omega_H)$, where ω_L and ω_H are the low- and high-tuning frequencies, respectively.

Strain Image

The local frequency vector is $\boldsymbol{\mu}(\mathbf{x},\mathbf{y},\mathbf{t})$, which is the component in the z direction that depends on the through-plane strain, and it can be computed with the following equation:

$$\boldsymbol{\mu}(\mathbf{x},\mathbf{y},\mathbf{t}) = \frac{\omega_L|I_L(x,y,t;\omega_L)| + \omega_H|I_H(x,y,t;\omega_H)|}{|I_L(x,y,t;\omega_L)| + |I_H(x,y,t;\omega_H)|}.$$

The local strain can then be computed with the following equation:

$$\varepsilon(x,y,t) = \frac{\omega_0}{\boldsymbol{\mu}(\mathbf{x},\mathbf{y},\mathbf{t})} - 1.$$

The computed strain is then used to color the image of the heart. Blue indicates no contraction, while red indicates contraction.

Acknowledgment: We thank Elizabeth A. Brady, RN, for recruitment and coordination.

References

1. Afridi I, Grayburn PA, Panza JA, Oh JK, Zoghbi WA, Marwick TH. Myocardial viability during dobutamine echocardiography predicts survival in patients with coronary artery disease and severe left ventricular systolic dysfunction. J Am Coll Cardiol 1998; 32:921–926.
2. Picano E, Sicari R, Landi P, et al. Prognostic value of myocardial viability in medically treated patients with global left ventricular dysfunction early after an acute uncomplicated myocardial infarction: a dobutamine stress echocardiographic study. Circulation 1998; 98:1078–1084.
3. Monin JL, Garot J, Scherrer-Crosbie M, et al. Prediction of functional recovery of viable myocardium after delayed revascularization in postinfarction patients: accuracy of dobutamine stress echocardiography and influence of long-term vessel patency. J Am Coll Cardiol 1999; 34:1012–1019.
4. Pierard LA, de Landsheere CM, Berthe C, Rigo P, Kulbertus HE. Identification of viable myocardium by echocardiography during dobutamine infusion in patients with myocardial infarction after thrombolytic therapy: comparison with positron emission tomography. J Am Coll Cardiol 1990; 15:1021–1031.
5. Marwick TH. The viable myocardium: epidemiology, detection, and clinical implications. Lancet 1998; 351:815–819.
6. Dilsizian V, Arrighi JA, Diodati JG, et al. Myocardial viability in patients with chronic coronary artery disease: comparison of 99m Tc-sestamibi with thallium reinjection and 18F fluorodeoxyglucose. Circulation 1994; 89:578–587.
7. Baer FM, Theissen P, Schneider CA, et al. Dobutamine magnetic resonance imaging predicts contractile recovery of chronically dysfunctional myocardium after successful revascularization. J Am Coll Cardiol 1998; 31:1040–1048.
8. Geskin G, Kramer C, Rogers WJ, et al. Quantitative assessment of myocardial viability after infarction by dobutamine magnetic resonance tagging. Circulation 1998; 98:217–223.
9. Lima JA, Judd RM, Bazille A, Schulman SP, Atalar E, Zerhouni EA. Regional heterogeneity of human myocardial infarcts demonstrated by contrast-enhanced magnetic resonance imaging: potential mechanisms. Circulation 1995; 92:1117–1125.
10. Kim RJ, Wu E, Rafael A, et al. The use of contrast-enhanced magnetic resonance imaging to identify reversible myocardial dysfunction. N Engl J Med 2000; 343: 1445–1453.
11. Axel L, Dougherty L. Heart wall motion: improved method of spatial modulation of magnetization for MR imaging. Radiology 1989; 172:349–350.
12. Zerhouni EA, Parish DM, Rogers WJ, Yang A, Shapiro EP. Human heart: tagging with MR imaging—a method for noninvasive assessment of myocardial motion. Radiology 1988; 169:59–63.
13. Guttman M, Prince JL, McVeigh ER. Tag and contour detection in tagged cardiac magnetic resonance images of the left ventricle. IEEE Trans Med Imaging 1994; 13:74–88.
14. Osman NF, Sampath S, Atalar E, Prince JL. Imaging longitudinal cardiac strain on short-axis images using strain-encoded MRI. Magn Reson Med 2001; 46:324–334.
15. Osman NF, McVeigh ER, Prince JL. Imaging heart motion using harmonic phase MRI. IEEE Trans Med Imaging 2000; 19: 186–202.
16. Garot J, Bluemke DA, Osman NF, et al. Fast determination of regional myocardial strain fields from tagged cardiac images using harmonic phase (HARP) magnetic resonance imaging. Circulation 2000; 101:981–988.
17. McVeigh ER, Atalar E. Cardiac tagging with breath-hold cine MRI. Magn Reson Med 1992; 28:318–327.
18. Kramer CM, Lima JA, Reichek N, et al. Regional differences in function within noninfarcted myocardium during left ventricular remodeling. Circulation 1993; 88:1279–1288.
19. Kramer CM, Rogers WJ, Theobald TM, et al. Remote noninfarcted region dysfunction soon after first anterior myocardial infarction: a magnetic resonance tagging study. Circulation 1996; 94:660–666.
20. Lima JA, Becker LC, Melin JA, et al. Impaired thickening of nonischemic myocardium during acute regional ischemia in the dog. Circulation 1985; 71:1048–1059.